Proceedings of ASME Turbo Expo 2020
Turbomachinery Technical Conference and Exposition
GT2020
June 22-26, 2020, London, England

GT2020-15018

EXPERIMENTAL AND KINETIC EVALUATION OF PRESSURIZED LEAN PREMIXED HYDROGEN-AIR FLAME STABILITY WITH CARBON DIOXIDE AND STEAM DILUTION

Jon Runyon[1†*], Daniel Pugh[1], Anthony Giles[1], Burak Goktepe[1], Philip Bowen[1], Richard Marsh[1†], Steven Morris[1]

[1]Cardiff University, Cardiff, Wales, United Kingdom
[†]ASME Member
[*]Corresponding author contact: RunyonJP@cardiff.ac.uk, +44 (0)2920 875931

ABSTRACT

A study has been undertaken to experimentally and numerically evaluate the use of carbon dioxide or steam as premixed fuel additive in hydrogen-air flames to aid in the development of lean premixed (LPM) swirl burner technology for low NO_x operation. Chemical kinetics modelling indicates that the use of CO_2 or steam in the premixed reactants reduces H_2-air laminar flame speed and adiabatic flame temperature within the well-characterized range of preheated LPM methane-air flames, albeit in markedly different proportions; for example, nearly 65 %vol CO_2 as a proportion of the fuel is required for a reduction in laminar flame speed to equivalent CH_4-air values, while approximately 30 %vol CO_2 in the fuel is required for an equivalent reduction in adiabatic flame temperature, significantly impacted by the increased heat capacity of CO_2. The 2nd generation high-pressure generic swirl burner, designed for use with LPM CH_4-air, was therefore utilized to experimentally investigate the influence of CO_2 and steam dilution on pressurized (up to 250 kW/MPa), preheated (up to 573 K), LPM H_2-air flame stability using high-speed OH chemiluminescence. In addition, exhaust gas emissions, such as NO_x and CO, have been measured in comparison with equivalent thermal power conditions for CH_4-air flames, showing that low NO_x operation can be achieved. Furthermore, pure LPM H_2-air flames are characterized for the first time in this burner, stabilized at low equivalence ratio (approximately 0.24) and increased Reynolds number at atmospheric pressure compared to the stable CH_4-air flame (equivalence ratio of 0.55). The influence of extinction strain rate is suggested to characterize, both experimentally and numerically, the observed lean flame behavior, in particular as extinction strain rate has been shown to be non-monotonic with pressure for highly-reactive and diffuse fuels such as hydrogen.*

Keywords: Hydrogen, Lean Premixed Combustion, Swirl Flame, Flame Stability, Extinction Strain Rate.

NOMENCLATURE

AFT	Adiabatic Flame Temperature
CCUS	Carbon Capture, Utilization, and Storage
CRZ	Central Recirculation Zone
GT	Gas Turbine
HPGSB-2	High Pressure Generic Swirl Burner (Mk. II)
LPM	Lean Premixed
NSD	Normalized Standard Deviation
SMR	Steam-Methane Reforming
II'_{OH*}	Instantaneous Integral OH* Intensity (a.u.)
II_{OH*}	Mean Integral OH* Intensity (a.u.)
P2	Burner Inlet Pressure (MPa)
P_{therm}	Thermal Power (kW)
r	Radial Direction (mm)
Re	Reynold Number
S_g	Geometric Swirl Number
S_L	Laminar Flame Speed (cm/s)
T2	Burner Inlet Temperature (K)
$\bar{u}$	Mean Nozzle Exit Axial Velocity (m/s)
y	Axial Direction (mm)
α	Thermal Diffusivity (m^2/s)
ΔP	Swirler Pressure Drop (% of *P2*)
κ_{ext}	Extinction Strain Rate (s^{-1})
φ	Equivalence Ratio

1. INTRODUCTION

Industrial gas turbine (GT) manufacturers have committed to increasing hydrogen capability in their engines from 20% (by volume) in natural gas by 2020 to 100% hydrogen by 2030, while also acknowledging the challenges associated with the combustion system related to this fuel shift away from natural gas [1]. In addition to the combustion challenge, the source of H_2 for these GTs is currently a source of contention, whether the H_2 is "grey" (produced via unabated natural gas reforming), "blue" (produced in conjunction with carbon capture, utilization, and storage, or CCUS), or "green"

(produced via electrolysis powered by renewable energy). Currently, 76% of H_2 produced globally comes from natural gas, with steam-methane reforming (SMR) the most prevalent technology employed [2]. The International Energy Agency [2] notes that the use of unabated SMR is expected to continue in the short term given favourable economics, however the push for decarbonization of H_2 production and the concentrated CO_2 by-product stream from SMR make combined SMR-CCUS applications viable under certain market conditions to produce "blue" H_2 in large quantities while large-scale, renewable "green" H_2 sources are further developed.

The potential for aligning industrial processes, such as SMR for H_2 production, with CCUS provides three distinct vectors (H_2, high purity CO_2, or steam generated from waste heat) for utilization in decarbonized gas turbine (GT) power generation, considering both new H_2-fired GTs and retrofit of existing GTs. Many GTs utilize dry low-NO_x burner technology based on the concept of swirl-stabilized lean premixed (LPM) operation for combustion of natural gas, however, research into the use of swirl-stabilized LPM operation for pure or dilute H_2 combustion is limited at conditions of elevated burner inlet temperature, *T2*, and inlet pressure, *P2*. For example, Stathopoulos et al. [3] evaluated steam dilution for NO_x abatement of CH_4-H_2-air swirl flames at *T2* = 673 K, *P2* up to 0.9 MPa, and thermal power, P_{therm}, up to 800 kW, however H_2 was limited to 10 %vol in CH_4. Mayer et al. [4] conducted flashback and lean blowoff stability trials at *T2* = 423 K, *P2* up to 0.5 MPa, and premixed H_2 up to 100 %vol fuel in blends with CH_4, noting in the conclusions that future studies should consider additional diluents to the fuel.

The higher reactivity and diffusivity of H_2 [5], compared with methane-based fuels, can lead to undesirable combustion phenomena in practical LPM systems, including flashback (due to increased flame speed) and high NO_x emissions (due to increased adiabatic flame temperature, AFT) [6,7]. To counteract these effects, a variety of approaches have been considered. In addition to the fuel injection strategies identified by Mayer et al. [4], Reichel et al. [6] investigated LPM swirl-stabilized H_2-air flames under elevated temperature and atmospheric pressure, utilizing axial air injection to improve the flashback performance of the burner while maintaining low NO_x emissions. Strakey et al. [8] found that H_2 addition up to 80 %vol in LPM natural gas extends the preheated, pressurized lean blowoff equivalence ratio, φ, which would in turn help to reduce NO_x emissions and flashback potential by reducing AFT and laminar flame speed (S_L), respectively. However, operation above 85% H_2 resulted in flashback issues using that particular swirl geometry under those conditions. Other measures taken to address these challenges in H_2 flames include non-premixed operation such as micromixing [9], high-momentum jets (e.g. FLOX) [10], or sequential combustion (e.g. Ansaldo Energia's GT-36) [11].

Fuel and/or oxidizer dilution can also be employed to control the reactivity and emissions formation of H_2 flames, as shown by Weiland and Strakey [12], who utilized excess N_2 for NO_x control of a H_2-air diffusion flame, and Tanneberger et al. [13] who utilized steam dilution for stoichiometric operation of non-premixed H_2-O_2 flames. However, both approaches imply air separation as part of the process, incurring an overall system efficiency penalty. If existing or new H_2 GTs are located near large-scale SMR H_2 production, and furthermore if CCUS systems are installed for CO_2 capture from the SMR process, then by-product streams of high-purity CO_2 or waste-heat generated steam would be potential available vectors for LPM H_2 fuel dilution. This may be particularly attractive to reduce downtime for retrofit on existing LPM GTs designed for use with natural gas, if compatibility can be demonstrated.

Canonical flame studies have been conducted previously with both CO_2 and steam dilution of H_2, however more practical studies are limited. Masri et al. [14] investigated piloted H_2-CO_2 fuel flames in the Sydney burner using a joint Raman-Rayleigh-LIF technique, noting that differential diffusion and the H radical play a role near lean extinction and also that CO_2 may react to give CO. A jet-stirred reactor study by Cong and Dagaut [15] supports this, concluding that H_2 oxidation was inhibited by decreased OH production in the presence of CO_2 as it reacts with H radicals, CO_2+H = CO+OH, when adding 30% CO_2 to a lean H_2-O_2-N_2 mixture at φ = 0.2. In studies evaluating steam dilution effects on S_L, both Kuznetsov et al. [16] and Lyu et al. [17] note a nonmonotonic pressure effect (increase followed by decrease with increasing pressure) in H_2-O_2 and H_2-air mixtures, respectively, with the effect in the latter observed up to 12%vol H_2O. This has been identified as related to the increased role of third body reactions such as $H+O_2$ (+M) = HO_2 (+M) with increasing pressure [16, 17]. Similar nonmonotonic behaviour of the extinction strain rate, κ_{ext}, as a function of pressure was observed by Niemann et al. [18] in a diffusion counterflow flame with H_2-N_2 fuel and air as oxidizer, influenced by the same third body reaction noted previously. Furthermore, in a more practical application, steam addition has been shown to limit NO_x emissions through both thermal and chemical pathways in premixed swirl combustion of high-H_2 content fuels under elevated temperature, atmospheric pressure conditions [19].

1.1 INVESTIGATION AIM

Given the recent resurgence in interest in H_2 use as a fuel for gas turbines alongside renewable power generation, there is a need for further validation of its use in practical LPM burner geometries operating at elevated *T2* and *P2*. To address this gap, this study presents experimental results at elevated temperature for both atmospheric and elevated pressure H_2-air, H_2-CO_2-air and H_2-H_2O-air flames. A detailed chemical kinetic study supplements the observed experimental measurements, particularly in regards to prediction of stable ignition and operating limits as well as the nonmonotonic pressure effect on pure and dilute H_2-air κ_{ext}. This study aims to identify and evaluate the influence of fuel diluent fraction and burner operating pressure on the lean stability and emissions of H_2-air swirl flames, accomplished primarily through the use of high-speed, time-resolved OH* chemiluminescence and exhaust gas analysis. This will inform future flame detection methods in H_2 GTs and provide a measure of heat release location for CFD model validation with detailed chemistry, given the relative simplicity of H_2 chemistry compared with gaseous hydrocarbons. By using LPM swirl burner technology, which is widely deployed for low-NO_x natural gas applications, the aim is to identify initial conditions required for retrofit of existing GTs to operate on H_2. The development of new, low-NO_x LPM H_2 combustor designs for use in GTs, a key development need for manufacturers by 2030 [1], will also be aided by the results of this study.

2. EXPERIMENTAL AND NUMERICAL APPROACH

2.1 GENERIC SWIRL BURNER

Atmospheric and elevated pressure combustion experiments were conducted in the 2nd generation high-pressure generic swirl burner HPGSB-2, seen in Fig. 1. The HPGSB-2 is well-characterized in terms of its stable operating limits, fuel flexibility, and emissions [20-23]. However, this study presents the first use of LPM pure and diluted H_2-air in this burner. Further information regarding this experimental setup can be found in other works [20-23]. The air mass flow rate was measured via Coriolis flow meter (Emerson CMF050) and then heated before fuel and diluent were injected upstream of the "Premixed Inlet" in Fig. 1, where *T2* (K-type, ±2.2 K) and *P2* (Druck PDCR 10/T, ±0.4%) were also measured. Fuel and diluent were metered as follows: CH_4 (Emerson CMF010), H_2 (Bronkhorst M14 mini CORI-FLOW), CO_2 (Emerson CMF025), and liquid H_2O (Bronkhorst M14 mini CORI-FLOW) into a steam generator. A radial-tangential swirler was used with a geometric swirl number of S_g = 0.8, with an 18 mm OD bluff-body lance within the exit nozzle. The swirler pressure drop, ΔP, was measured with a Druck PDCR 10/35L differential pressure transducer (0.04% full scale to 70 kPa). The burner assembly was installed in a high-pressure optical chamber, which allows visual access using quartz windows and a cylindrical quartz burner confinement [20].

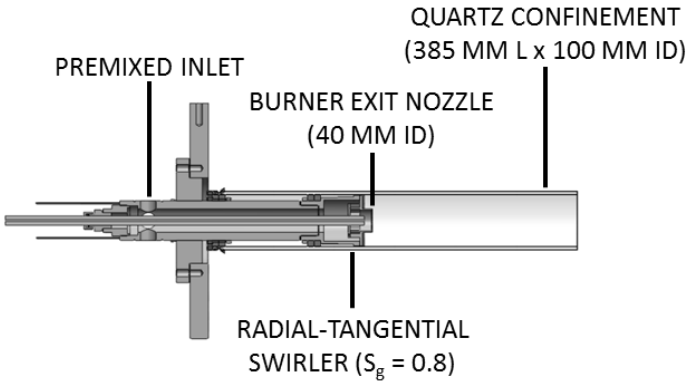

Figure 1. SECTIONED VIEW OF HPGSB-2

2.2 EXPERIMENTAL CONDITIONS

All combustion studies were conducted under LPM conditions, with two distinct pressure scalings and burner inlet temperatures: 125 kW/MPa at *T2* = 523 K ± 5 K and 250 kW/MPa at *T2* = 573 K ± 5 K, respectively. Thus, atmospheric pressure experiments, to be discussed first, were conducted at P_{therm} = 12.5 kW at 532 K, followed by selected pressurized conditions presented at each scaling given above. Utilizing this scaling method maintains volumetric flow, thus bulk exit velocity from the swirler nozzle, $\bar{u}$, for constant φ and diluent fraction as *P2* is increased.

For both CH_4-air and H_2-based flames, the lean operational limit was characterized by flame detachment from the burner exit nozzle and the rich operational limit was characterized by intermittent flame flashback into the burner exit nozzle. Both phenomena were identified by in-situ monitoring of the high-speed OH* chemiluminescence images. The lean stability limit was identified by intermittent loss of the flame root attached to the burner exit nozzle resulting from small increments in either inlet air (at a fixed fuel dilution rate) or diluent flow (with fixed φ). The flashback stability limit was characterized by momentary upstream flame retreat into the burner exit nozzle observed with reduction of inlet air or diluent flow. Neither CH_4 nor H_2 flame was driven to LBO (to prevent build-up of unburned fuel in the exhaust) or full flashback (to prevent damage to upstream burner components), both of which are particularly critical for the H_2 cases at elevated pressure.

Table 1 provides the experimental conditions employed in this study. For the dilute H_2 conditions, the premixed fuel dilution rate is presented as "%vol H_2O Fuel" and "%vol CO_2 Fuel" per Equations 1.a and 1.b, respectively. For example, the designation "$50H_2$–$50CO_2$" represents an equal molar concentration of H_2 and CO_2 in the full premixed reactants. The swirler pressure drop, ΔP, is presented as a percentage of *P2* with the highest pressure drop observed for the 250 kW/MPa condition with H_2-CO_2 fuel.

Table 1. EXPERIMENTAL CONDITIONS IN THE HPGSB-2

Fuel	T2 (± 5 K)	P2 (MPa)	P_{therm} (kW)	φ	ΔP (%)
CH_4	523	0.11	12.5	0.49 - 0.80	0.1 - 0.3
H_2	523	0.11	12.5	0.21 - 0.25	0.8 - 1.1
H_2-H_2O	523	0.11 - 0.15	12.5 - 18.75	0.25 - 0.35	0.6 - 0.9
H_2-CO_2	523 - 573	0.11 - 0.275	12.5 - 68.75	0.25 - 0.40	0.7 - 4.5

$$\%vol\ H_2O\ Fuel = \frac{(\%vol\ H_2O)_{premix}}{(\%vol\ H_2O)_{premix}+(\%vol\ H_2)_{premix}} \quad (1.a)$$

$$\%vol\ CO_2\ Fuel = \frac{(\%vol\ CO_2)_{premix}}{(\%vol\ CO_2)_{premix}+(\%vol\ H_2)_{premix}} \quad (1.b)$$

2.3 EXPERIMENTAL DIAGNOSTICS

2.3.1 TIME-RESOLVED OH* CHEMILUMINESCENCE

Time-resolved OH* chemiluminescence images were captured for each experimental condition system at 90° relative to the axial flow direction. Measurements focused on the well-known $A^2\Sigma^+$–$X^2\Pi$ OH* peak at 309 nm [24] using a 315 nm (±15 nm FWHM) bandpass filter. This ultraviolet system was selected due to the limited visible spectra emitted by the dilute H_2 flames, as normal visible bands available in CH_4-air flames resulting from CH*, C_2*, and broadband CO_2* emission are not present in H_2-air and H_2-H_2O-air flames and are very limited to certain dilution rates for H_2-CO_2-air flames.

OH* measurements were made with an intensified high-speed CMOS camera system as detailed in [21]. The system was operated at 4000 Hz, with an intensifier gate time of 10 μs and constant gain. The image resolution of 4.6 pixels/mm results in a field of view of 75 mm (axial, *y*) x 100 mm (radial, *r*) relative to the edge and centreline of the burner exit nozzle, respectively. For averaged images, each instantaneous OH* chemiluminescence image was filtered using a 3x3 pixel median filter and background-corrected before being temporally-averaged from 2000 images. The temporally-averaged images were then processed using an Abel inversion algorithm [20]. Temporal variation of the OH* chemiluminescence signal was evaluated using a pixel-wise normalized standard deviation (NSD, equal to the quotient of

pixel intensity standard deviation and mean pixel intensity) calculated from each set of 2000 instantaneous images, where unity values indicate regions of high intensity fluctuation. Mean and instantaneous integral intensity, II_{OH^*} and II'_{OH^*} [20] respectively, were also evaluated.

2.3.2 EXHAUST GAS ANALYSIS

Exhaust gas sampling and analysis were conducted using an industry standard system detailed in [21-23], with the addition of CO measurements. Total NO_x concentrations were measured hot and wet to avoid any losses, with data presented at the equivalent dry conditions using an equilibrium H_2O molar fraction from Chemkin-Pro [25]. For CO measurements, a chiller reduces the exhaust molar H_2O concentration to < 1%. Dry CO concentrations were measured using a nondispersive infrared analyzer (Signal Instruments 9000MGA), calibrated in the range 0-904 ppmV. Both NO_x and CO emissions were normalized to 15% O_2 concentration as in [21], using exhaust molar O_2 measurements. Typical uncertainty of ~5% of measurement accounts for analyzer specifications, linearization, and accuracy in span gas certification.

2.4 CHEMICAL KINETICS MODELLING

A parametric chemical kinetics modelling study was conducted using Chemkin-Pro [25] to supplement the observed experimental phenomena. Two reaction mechanisms were used: GRI-Mech 3.0 [26] for CH_4-air and the H_2 mechanism from Li et al. [27] for all H_2-based conditions with N_2 as the bath gas. The equilibrium program was used to model AFT and equilibrium exhaust H_2O concentrations for use in normalizing wet emissions measurements to equivalent dry conditions [22]. The PREMIX program was used to calculate laminar flame speeds, S_L, based on a freely propagating flame model. Solutions in this model were based on an adaptive grid of 1000 points, with mixture-averaged transport properties and trace series approximation. Finally, the OPPDIF program was used to evaluate κ_{ext} for consideration in its use as a predictor of lean flame stability and flame stabilization location [28]. The model was based on twin premixed fuel/air jets in opposition and included the use of multi-component diffusion coefficients and Soret effects. This is similar to the method used by Shanbhogue et al. [28] in a burner of similar swirl geometry (S_g = 0.7 [28] vs 0.8 in this work), Reynolds number ($2x10^4$ [28] vs $1.5x10^4$-$2x10^4$) and up to 20% H_2 in CH_4.

3. RESULTS AND DISCUSSION

3.1 CHEMICAL KINETICS MODELLING

3.1.1 ATMOSPHERIC PRESSURE

Given that the HPGSB-2 was designed for use with CH_4, the initial chemical kinetic study undertaken aimed to identify an appropriate dilute H_2 blend to allow for successful LPM ignition. This was accomplished by identifying the fuel diluent concentration required to reduce the laminar flame speed, S_L, of the H_2 blend within the stable ignition range for LPM CH_4-air at φ = 0.6 with $T2$ = 523 K and $P2$ = 0.11 MPa. The results are shown in Fig. 2. The dilution rate required for LPM ignition at similar S_L to CH_4-air flames is approximately $35H_2$-$65CO_2$ and $30H_2$-$70H_2O$, respectively.

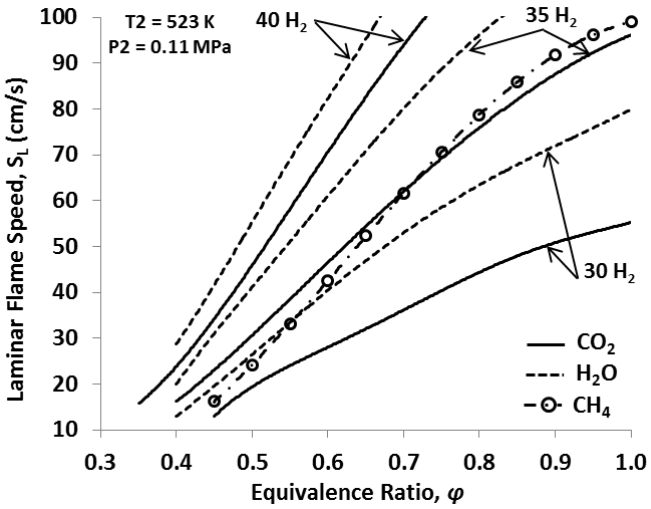

Figure 2. S_L OF CH_4-AIR, H_2-CO_2-AIR, AND H_2-H_2O-AIR MIXTURES WITH VARYING DILUENT CONTENT

Other important trends are also identified: 1) S_L of H_2O dilute H_2-air flames is consistently higher than with CO_2 dilution and 2) the rate at which S_L decreases with increasing dilution is more evident with CO_2 dilution than with H_2O dilution. This second trend suggests that stable operation at higher equivalence ratios may be possible with CO_2 dilution, therefore yielding the benefits of reduced excess air (and thus N_2 content for NO_x formation) along with increasing the product CO_2 concentration for potential recovery via CCUS.

Furthermore, as will be discussed in Section 3.2.1, pure and dilute H_2-air swirl flames could be stabilized below φ = 0.3, which appears to be very near the convergence limit of the Li et al. [27] mechanism, underscoring the catalytic influence that turbulence and diffusivity have on swirl flame stabilization which cannot be captured by the laminar flame model. This also highlights a limitation of the mechanism in regards to ultra-lean, highly dilute H_2 mixtures.

The parametric chemical kinetic modelling study was further expanded to evaluate the influence of fuel diluent fraction on key stability and emissions indicators: S_L, AFT, and κ_{ext} for all lean equivalence ratios ($\varphi \leq 1$) at $T2$ = 523 K and $P2$ = 0.11 MPa. The results are presented in Fig. 3, with S_L, AFT, and κ_{ext} plotted against %Fuel Diluent for CO_2 (a, b, and c, respectively) and H_2O (d, e, and f, respectively). Similar to the approach taken in Fig. 2, reference values are also plotted for a CH_4-air flame without dilution at a stable burner operating condition (φ = 0.6), specifically S_L = 42.6 cm/s, AFT = 1834 K, and κ_{ext} = 329 s^{-1}. The trend observed in Fig. 2, namely the reduction rate in S_L with increased CO_2 dilution compared with H_2O dilution, is more evident in Figures 3.a and 3.d, particularly above 60% Fuel CO_2 and φ = 0.5. To achieve the same S_L as the CH_4-air flame at φ = 0.6, a pure H_2-air flame would have to be operated slightly above φ = 0.3, while 66% Fuel CO_2 and 69% Fuel H_2O dilution would be required to achieve the same S_L at φ = 0.6. This represents almost an order of magnitude reduction in S_L from the pure H_2-air S_L at φ = 0.6, which emphasizes the reactivity of lean H_2-air flames, even at high dilutions rates. A similar trend regarding the rate of reduction of AFT is observed in Figures 3.b and 3.e, with CO_2 dilution shown to increase the rate of reduction compared with H_2O, particularly above φ = 0.6.

Whereas quite high (>65%) H_2 dilution would be required for an equivalent reduction in S_L to CH_4-air values, significantly less diluent is required for an equivalent reduction in AFT, namely 33% Fuel CO_2 and 37% Fuel H_2O at φ = 0.6. This is due mainly to the increased specific heat capacity of CO_2 relative to steam and N_2, 21% and 34% higher at 523 K, respectively. This difference between dilution rates for reduction in H_2-air S_L and AFT to CH_4-air values suggests that modifications to the burner operating regime or design may be required to achieve useful burner exit temperatures while avoiding flashback. This would include higher total mass flow rate through the burner, resulting in higher $\bar{u}$, to the potential detriment of increased ΔP, as shown in Table 1, unless burner geometry is redesigned. To enable more straightforward retrofit applications, operation of H_2-based fuels at lower thermal power (e.g. part load) may be required to maintain existing burner geometry and design ΔP.

Finally, κ_{ext} modelling is presented in Figures 3.c and 3.f, showing a stronger dependence on φ than S_L, with pure H_2-air κ_{ext} reducing nearly three orders of magnitude from φ = 1.0 to φ = 0.3. This fundamental parameter has been used to identify CH_4-H_2 flame stabilization regimes for lean operation in highly strained, turbulent flows [28]. The application of this technique is extended here to consider if κ_{ext} of ultra-lean pure and dilute H_2-air can be utilized to indicate flame stability, in particular as Hu et al. [29] have identified that high H_2-content fuels exhibit negative Markstein lengths under LPM conditions. Negative Markstein lengths indicate an increase in H_2 flame speed with increasing stretch rate. This behaviour is noted as being impacted significantly by preferential fuel diffusion under lean conditions [29].

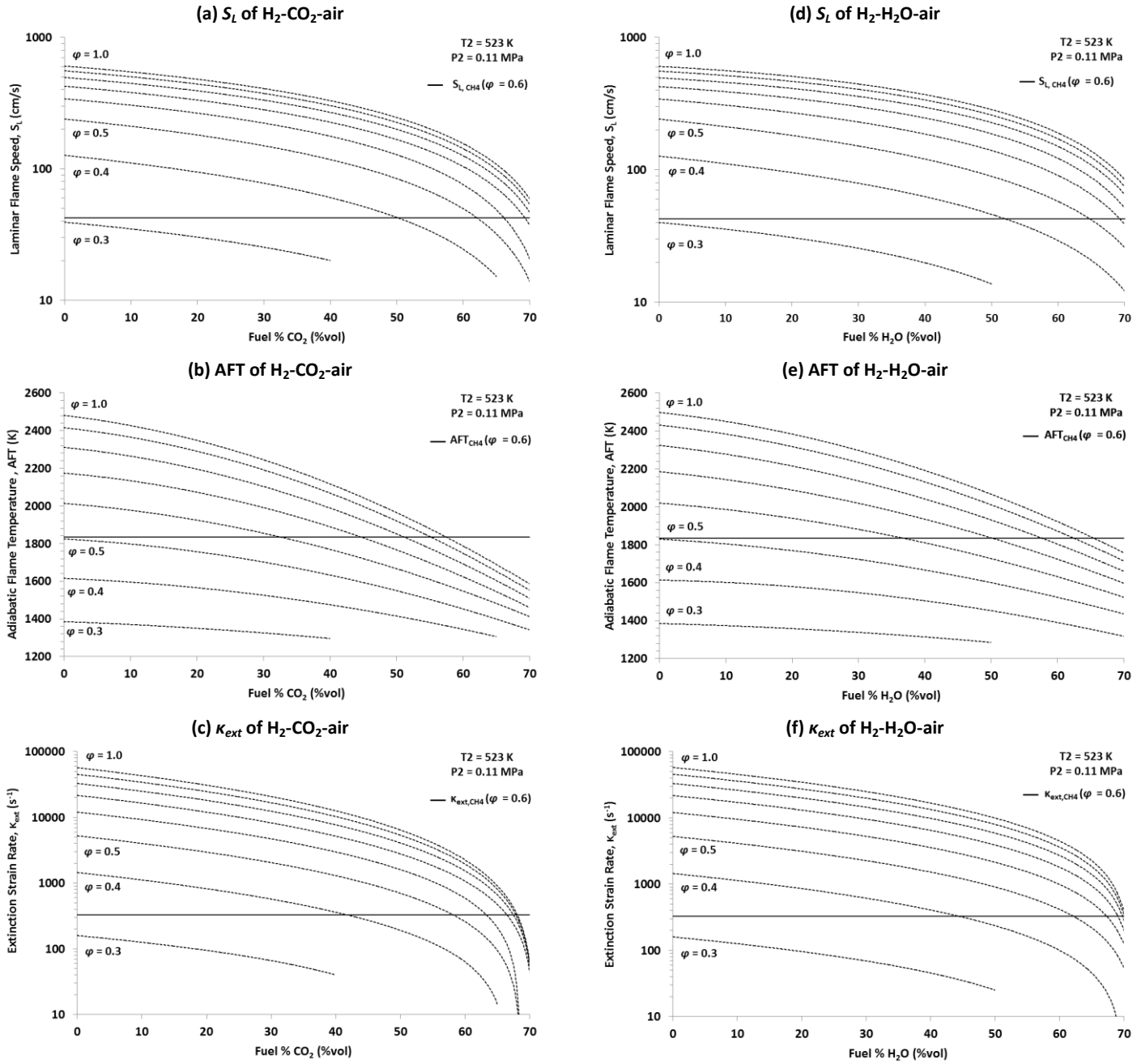

Figure 3. INFLUENCE OF H_2 FUEL DILUTION ON MODELLED S_L, AFT, AND κ_{ext}

In general, κ_{ext} is higher for the H_2O-diluted cases than the CO_2-diluted cases. Similar behaviour between S_L and κ_{ext} is seen in regards to reduction rate with diluent addition, with 63% Fuel CO_2 and 67% Fuel H_2O required to achieve an equivalent reduction to CH_4-air values at φ = 0.6. The similarities in fuel dilution effects on S_L and κ_{ext} are to be expected as the simple strained flame extinction is driven by a chemical timescale that incorporates both S_L and the gas thermal diffusivity, α, which was included in the κ_{ext} calculation (Soret effects) with $\alpha_{CO2} < \alpha_{H2O}$ at *T2* = 523 K [30].

3.1.2 ELEVATED PRESSURE

The chemical kinetic modelling of κ_{ext} was broadened to consider elevated pressure effects, particularly given the elevated pressure LPM conditions explored in this study and the experimental observations by Niemann et al. [18] discussed in Section 1. Whereas Niemann et al. [18] measured and modelled κ_{ext} for diffusion H_2-N_2-air counterflow flames, the modelling presented in Fig. 4 incorporates pure and dilute (50 %vol Fuel Diluent) LPM H_2-air and CH_4-air at *T2* = 523 K and φ = 0.6. A similar nonmonotonic trend is observed here, with maximum κ_{ext} for pure H_2-air at 0.7 MPa. This maximum peak reduces by an order of magnitude in the dilute H_2 cases, while also shifting to lower pressures, 0.2 MPa for H_2O and 0.125 MPa for CO_2. This shift in κ_{ext} is expected to influence lean flame stabilization when increasing burner operating pressure, and suggests that the flame may stabilize in different regions of aerodynamic strain within the flow field, critical for avoiding flame flashback during GT operation with H_2-based fuels.

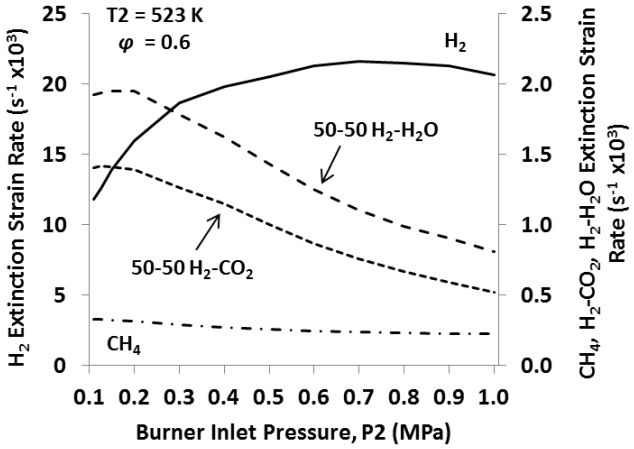

Figure 4. κ_{ext} AS A FUNCTION OF BURNER PRESSURE

3.2 SWIRL FLAME STABILITY AND EMISSIONS

3.2.1 ATMOSPHERIC PRESSURE STABILITY (12.5 kW)

Burner operation was first examined at atmospheric pressure (*P2* = 0.11 MPa), elevated temperature (*T2* = 523 K), and constant fuel flow (P_{therm} = 12.5 kW). To identify the influence of H_2 dilution on flame stability, two parametric operations were undertaken individually. First, diluent flow in the premixed reactants was varied at a fixed φ until either flame liftoff or intermittent flashback was observed, or in very lean cases, the diluent flow could be reduced completely to yield a pure H_2-air flame. Second, at selected fixed dilution ratios, φ was varied by manipulating the air flow. These operations yield the stability curves and stability map shown in Figures 5.a and 5.b, respectively.

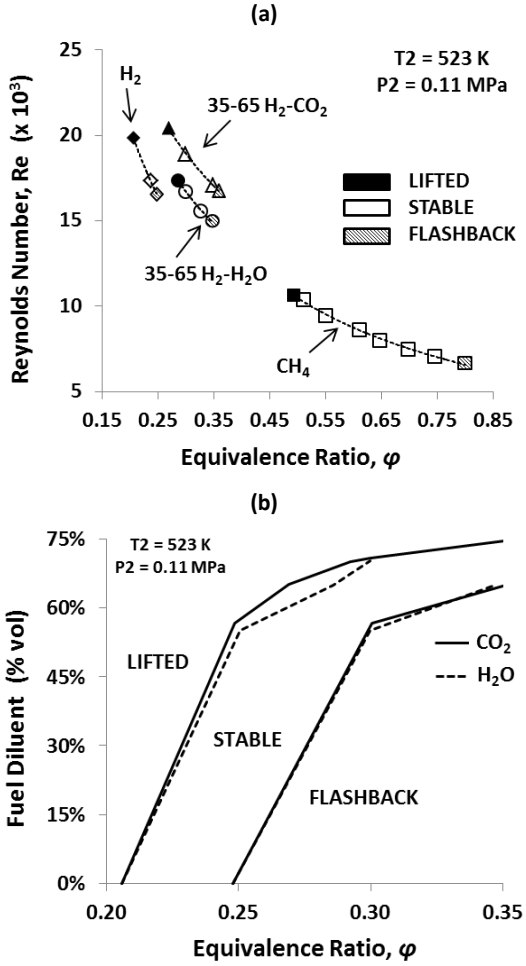

Figure 5. 12.5 kW FLAME STABILITY MAPS AS A FUNCTION OF φ AND (a) REYNOLDS NUMBER (CLOSED = LIFTED, OPEN = STABLE, HASHED = FLASHBACK) OR (b) % FUEL DILUENT

In Figure 5.a, the 35-65 H_2-diluent blend, identified by chemical kinetic modelling (see Section 3.1.1) to yield similar S_L and κ_{ext} to an equivalent CH_4-air flame, is used as a basis to emphasize the influence that H_2 has on flame stability, even under highly dilute conditions. Stable operation in this burner requires higher bulk flow through the burner, and thus higher exit velocities from the swirler nozzle, when replacing CH_4 with H_2. This results in a stable flame $\bar{u}$ that is approximately twice ($\bar{u}$ = 15-20 m/s) that for a stable CH_4-air flame ($\bar{u}$ = 6-9 m/s), and thus the stable Reynolds number (*Re*) doubles as well. The stable operating window is also affected by H_2 replacement, both narrowing and shifting to leaner φ as compared with the CH_4-air flame. As seen in both Figures 5.a and 5.b, operation with CO_2 diluent extends the stable operating range of H_2 flames compared with pure H_2-air and steam-diluted H_2-air. This is influenced particularly by the increased dynamic viscosity of CO_2 compared to H_2O at these conditions, which serves to increase levels of turbulence (e.g. *Re*) for the same $\bar{u}$, enhancing H_2 flame propagation. Operation with pure H_2-air was achieved, bounded by a detached flame at φ = 0.206 and intermittent flashback at φ = 0.248. At this low thermal power, burner exhaust temperatures measured < 1000 K for H_2-based flames, influenced by the high dilution levels and heat losses to the experimental rig, evidenced by CH_4-air flame exhaust temperature at the highest equivalence ratio (φ = 0.8),

which measured only about 200 K higher. Furthermore, as described by Amato et al. [31], high CO_2 and H_2O dilution at low operating pressure will enhance radiative heat losses compared with O_2 or N_2. Initial studies at higher P_{therm} (25 kW) for atmospheric pressure conditions suggest extension of the H_2-air stable operating range. This is attributed to increased $\bar{u}$ as a result of increased mass flow, which makes the flame more resistant to flashback and also results in elevated burner exit temperatures, however ΔP is increased. This will be the subject of future study.

As shown in Fig. 5b, for increasing φ, the achievable CO_2 or H_2O dilution increases, as the increased H_2 flame speed is offset by the physical and chemical effects of the diluents, however the stable operation range narrows. In both the CO_2 and steam dilution cases, the widest operating range is achieved at φ = 0.25, which is therefore selected for pressurized conditions detailed in Sections 3.2.2 and 3.2.3.

Abel-transformed OH* chemiluminescence images are presented in Fig. 6 for selected stable conditions plotted in Fig. 5.a. The Abel transformation is based on an assumption that the flame is axisymmetric about the burner centreline, thus for simplicity, only one half of the flame is shown (with flow from bottom to top) and the false colormap normalized to the maximum for each individual image. Figure 6.a provides a reference CH_4-air flame at φ = 0.6, as used in the chemical kinetics modelling, along with three stable H_2-based flames: pure H_2-air (Fig. 6.b), $35H_2$-$65CO_2$ (Fig. 6.c) and $35H_2$-65H2O (Fig. 6.d), with the conditions selected at near-equivalent bulk exit velocity, $\bar{u}$ = 17.7 m/s ±2%. All flames are seen to stabilize along the shear layer of low axial velocity between the CRZ and outer recirculation zone, as has been shown previously for this burner [20].

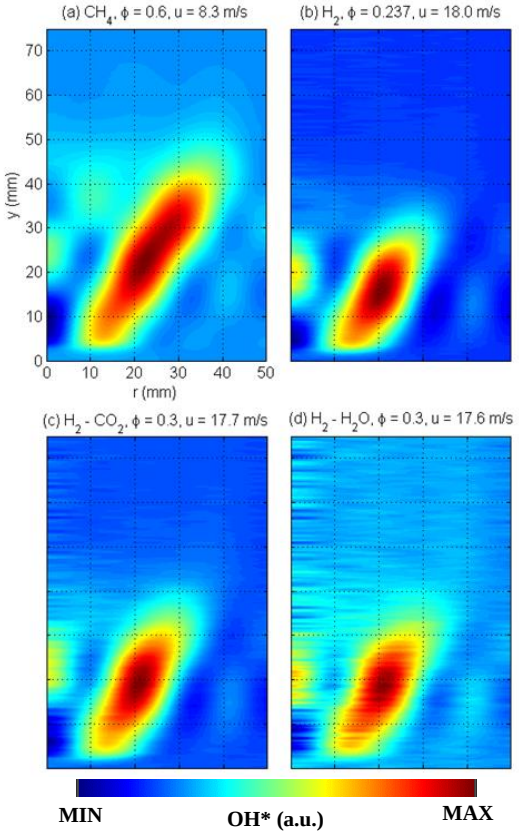

Figure 6. ABEL-TRANSFORMED OH* OF STABLE 12.5 kW FLAMES: (a) CH_4, (b) H_2, (c) $35H_2$-$65CO_2$ and (d) $35H_2$-$65H_2O$

Even under high amounts of air and premixed reactant dilution, the H_2-based flames are significantly more compact than the CH_4-air flame; this is despite the chemical kinetics modelling predicting lower S_L, AFT, and κ_{ext} for these conditions. These predictions would imply lower reactivity than the CH_4-air flame, however, do not necessarily account for the influence of increased turbulence and diffusivity, resulting in an increased flame propagation speed as the H_2-based flame is subjected to increased stretch, as shown by Hu et al. [29].

Both dilute H_2-air flames have a similar bulk shape, slightly less compact than the pure H_2-air flame, however the flames vary significantly in terms of absolute OH* intensity, as seen in Fig. 7. Figure 7 provides a moving average (period = 20 samples) plot of the time-varying OH* integral intensity, II'_{OH*}, for 2000 images along with the mean OH* integral intensity, II_{OH*}, calculated for each dataset. These flame images were captured at the H_2-based conditions in Fig. 6. These quantities have been shown to be good qualitative measures of LPM flame heat release [20], and the time-varying signal can provide indications of flame instabilities (e.g. localized extinction may result in a reduction in II'_{OH*}).

It should be noted that CH_4-air II_{OH*} at φ = 0.6 is an order of magnitude higher than the pure H_2-air values here given the higher AFT and contribution from broadband CO_2* chemiluminescence, which may also be contributing in the H_2-CO_2 case. The reduction in II'_{OH*} from pure H_2-air to H_2-CO_2 to H_2-H_2O is suggested in the first instance related to a reduction in heat release with CO_2 dilution, and this corresponds to a measured reduction in the burner exit temperature. However, the reduction in II'_{OH*} from H_2-CO_2 to H_2-H_2O was more surprising, given that H_2-H_2O AFT is 38 K higher than H_2-CO_2 AFT under these conditions and measured exhaust temperatures were also higher. This suggests that the production of OH* may be chemically limited in the H_2-H_2O case, and warrants further investigation.

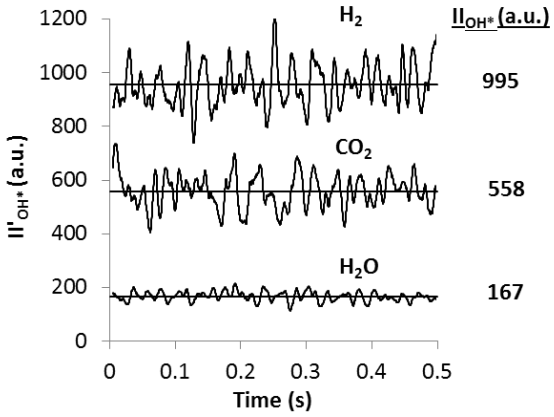

Figure 7. MOVING AVERAGE PLOT OF TIME-VARYING II'_{OH*} FOR PURE AND DILUTE H2-AIR FLAMES (FROM FIG. 6) WITH MEAN II_{OH*} PLOTTED FOR ORIGINAL RAW DATA

In contrast to the spatially-integrated II'_{OH*} measurement, the NSD plot provides spatial resolution of the temporally-varying OH* chemiluminescence intensity fluctuation, which is of particular importance for identifying flame liftoff from the burner exit nozzle. The NSD plot provides a measure of OH* intensity stability. For example, intermittent flame detachment from the swirler exit nozzle would subject the pixels in that region to high intensity

fluctuations, thus increasing the collated pixel standard deviation relative to the mean pixel intensity. This is evident in Fig. 8 which provides NSD plots for one-half of the pure H_2-air flames. Figure 8.a is calculated from the stable condition at φ = 0.237 (refer to corresponding time-averaged image in Fig. 6.b), Fig. 8.b is calculated from the lifted flame condition at φ = 0.206, and Fig. 8.c is calculated as the lifted flame image NSD normalized to the stable flame image NSD. It must be noted that these plots are formed from the instantaneous, background-corrected OH* chemiluminescence images and as such are line-of-sight integrated, which gives a bulk conical flame appearance for this swirl burner rather than the pseudo-planar representation resulting from Abel-transformation in Fig. 6. A near-unity value in Figures 8.a and 8.b suggest regions of high OH* intensity fluctuation as the standard deviation approaches or, in some cases, exceeds the mean value.

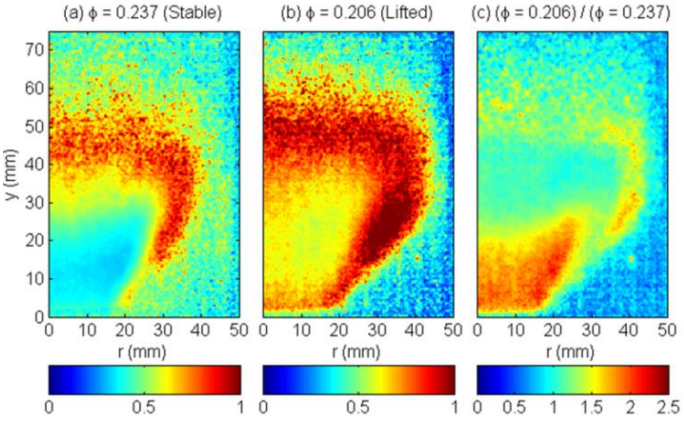

Figure 8. NSD PLOTS OF OH* FOR (a) STABLE AND (b) LIFTED H_2-AIR FLAMES, WITH (c) SHOWING (b) NORMALIZED TO (a)

In the stable H_2-air flame case of Fig. 8.a, the regions near the burner exit nozzle (y = 0 mm) show relatively low fluctuation, which is in agreement with the Abel-transformed image of Fig. 6.b. The highest fluctuation levels in the stable case occur along the outer shear layer, which is expected given the influence of vortex shedding from the burner nozzle and influence from the outer recirculation zone (further flow field information for this particular swirler in other works [20, 21]), both highly turbulent regions where the LPM H_2 flame may exist given its stretched flame response. As the flame moves towards the lifted condition with an increase in air mass flow, the NSD plot of Fig. 8.b is markedly different, showing high OH* intensity fluctuations in the region near the burner exit and expanding influence from the outer recirculation zone as the flame moves further downstream. To quantify the change in OH* intensity fluctuation in the lifted condition, the normalized NSD plot in Fig. 8.c. details the regions within the flow field where intensity fluctuations are occurring, notably up to 2.5 times the normalized stable OH* fluctuation occurs when moving from stable to lifted flame configuration in the region within 20 mm axially and radially of the burner exit.

This technique is applied further to evaluate the resistance of dilute H_2-air flames to lean flame detachment, with results for $35H_2$-$65CO_2$ and $35H_2$-$65H_2O$ presented in Fig. 9. The NSD plots of Fig. 9.a and 9.b are calculated from the lifted flame conditions plotted as closed symbols in Fig. 5.a and the plots of Fig. 9.c and 9.d are normalized relative to the pure H_2-air lifted flame NSD plot in Fig. 8.b.

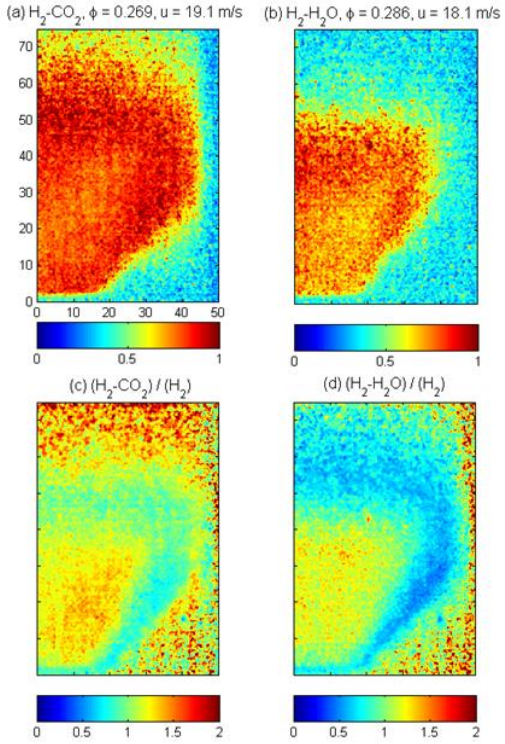

Figure 9. NSD PLOTS OF OH* FOR (a) $35H_2$-$65CO_2$ AND (b) $35H_2$-$65H_2O$ LIFTED FLAMES, WITH (c) AND (d) NORMALIZED TO THE H_2-AIR PLOT IN FIG. 8.b.

Whereas the stable flame shapes for the corresponding $35H_2$-$65CO_2$ and $35H_2$-$65H_2O$ flames are nearly identical in Figure 6.c and 6.d, respectively, the flame response under detached conditions is strikingly different. The $35H_2$-$65CO_2$ lifted flame (Fig. 6.a) has an almost uniform high intensity fluctuation spanning the flow field from the burner exit nozzle, along the shear layer, and across the central recirculation zone. Some influence from the outer recirculation zone can also be seen with the start of an M-shaped flame. In the $35H_2$-$65H_2O$ lifted flame (Fig. 6.b), the intensity fluctuations are also observed to cover the flow field, however this region is more compact than the H_2-CO_2 flame while also generally lower in intensity, particularly along the shear layer. Under these conditions, κ_{ext} is expected to be higher for the $35H_2$-$65H_2O$ flame than the $35H_2$-$65CO_2$ flame, as flame liftoff for the H_2-H_2O flame occurs at φ = 0.286 compared with φ = 0.269 for the H_2-CO_2 flame, which may act to suppress flame fluctuations as the flame approaches detachment and stabilizes within the flow field rather than along the bluff body/exit nozzle. While it may dampen the fluctuations, increased κ_{ext} cannot keep the H_2-H_2O flame attached to the burner exit nozzle, as turbulence levels are nearly 15% lower in the H_2-H_2O lifted case (due mainly to differences in dynamic viscosity between H_2O and CO_2), thereby reducing H_2 turbulent flame speed. Normalization by the pure H_2-air lifted NSD plot (Fig. 8.b) indicates that both H_2-CO_2 and H_2-H_2O flames are subject to more fluctuation under lifted conditions, with the H_2-CO_2 lifted case showing highest fluctuations in the central core, which could be expected given the high Re and expected low κ_{ext} relative to the other flames.

3.2.2 EXHAUST GAS EMISSIONS

Given the low AFT of the ultra-lean conditions investigated, the thermal NO_x formation pathway is effectively reduced, in addition to the reduction of premixed N_2 concentration with CO_2 or H_2O addition. The lack of hydrocarbons also eliminates the prompt NO_x pathway, as highlighted by Glarborg et al. [32]. Given the suppression of thermal and prompt NO_x pathways under these conditions, it is expected that the N_2O and NNH pathways contribute, particularly with increasing pressure [32]. Measured NO_x emissions could be achieved at the 125 kW/MPa scaling, with total NO_x (combined NO and NO_2) < 1 ppm in H_2-CO_2 cases and < 2 ppm across all other experimental conditions. However, high CO emissions were measured at low AFT in the H_2-CO_2 cases with high CO_2 dilution as shown in Fig. 10. While a similar trend could be expected for LPM CH_4-air flames with reduction in AFT [33], the mechanism for CO formation differs from incomplete hydrocarbon oxidation and is instead attributed to the CO_2+H=CO+OH reaction, similar to that suggested by Glarborg and Bentzen [34] for high CO_2-dilution of CH_4-oxyfuel combustion.

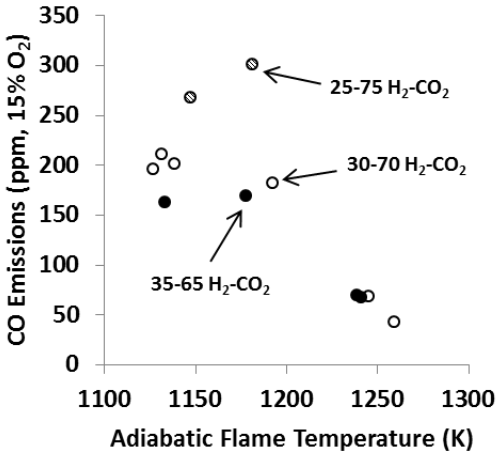

Figure 10. CO EMISSIONS FROM H_2-CO_2 12.5 kW FLAMES

3.2.3 ELEVATED PRESSURE (125 kW/MPa Scaling)

As the burner pressure is increased, the associated increase in premixed reactant density is offset by an increase in mass flow to maintain a similar bulk flow profile. By holding φ constant at 0.25, it is therefore possible to evaluate flame stability as a function of the dilution rate. Abel-transformed images of stable $55H_2$-$45CO_2$ and $55H_2$-$45H_2O$ flames at *P2* = 0.15 MPa are shown in Figures 11.a and 11.c, respectively, along with lifted flame NSD plots for increasing diluent content at the same *P2*. For the stable flame conditions, a comparison can be made between Figures 11.a and 6.c (H_2-CO_2) as well as Figures 11.b and 6.d (H_2-H_2O), noting the similar flame stabilization location along the outward expanding shear layer. Similar reactivity between these two different operating conditions, 1) 35% H_2 at φ = 0.3 in Fig. 6 and 2) 55% H_2 at φ = 0.25 in Fig. 11, might be expected given the nominally equal AFT and $\bar{u}$ for each diluent (S_L and κ_{ext} could not be modelled at these conditions). In the H_2-CO_2 case, the AFT in Fig. 6.c is 1178 K compared to 1180 K in Fig. 11.a. In the H_2-H_2O case, the AFT in Fig. 6.d is 1215 K compared to 1197 K in Fig. 11.a. The value of $\bar{u}$ increases by ~4% to 18.4 m/s between these conditions.

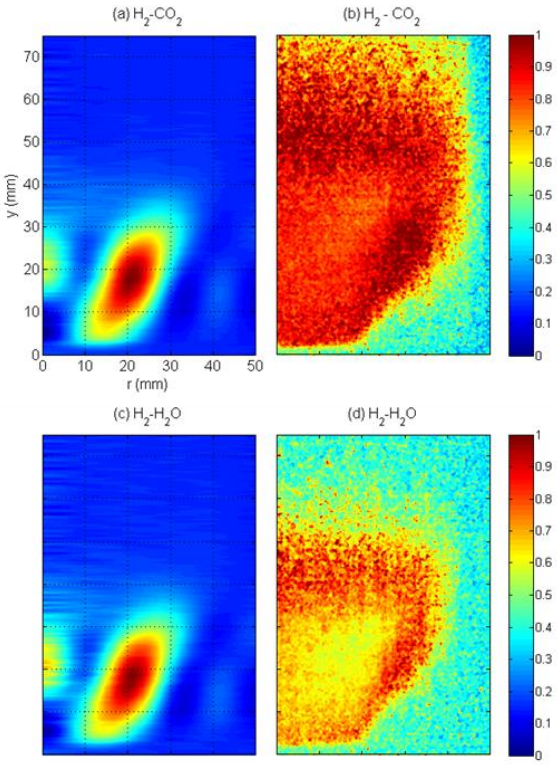

Figure 11. ABEL-TRANSFORMED OH* FOR STABLE (a) $55H_2$-$45CO_2$ and (c) $55H_2$-$45H_2O$ FLAMES AT φ = 0.25, *P2* = 0.15 MPa. ASSOCIATED NSD PLOTS (b, d) FOR LIFTED FLAMES WITH INCREASED DILUTION.

Despite the similar AFT and $\bar{u}$, the flame brush is observed to be more compact at *P2* = 0.15 MPa than at atmospheric conditions in Fig. 6. For example, the 50% OH* intensity contour (blue-green), extends beyond *y* = 40 mm in Fig. 6 for both diluents, however in Fig. 11, this contour extends just beyond *y* = 30 mm. This is attributed to two key factors. First, the relatively low $\bar{u}$ is not sufficient to balance the increasing flame propagation speed as turbulence increases with pressure using this flow scaling method (due to the reduction in premixed reactant dynamic viscosity, thus increasing *Re*). Second, as highlighted by the chemical kinetic modelling, it is expected that κ_{ext} would increase with a relatively small change in pressure for these dilution rates. Thus, the thermodiffusive effects allow for flame stabilization in this region of increased turbulence. This is further supported by considering the NSD plots in Figures 11.b and 11.d for H_2-CO_2 and H_2-H_2O, respectively.

In both cases, the maximum dilution to achieve flame detachment increased over the equivalent φ = 0.25 condition at atmospheric pressure, with increased turbulence and thermodiffusive effects balancing the reaction limiting physical and chemical effects of dilution. Maximum CO_2 fuel dilution increased from 56.7% to 57.5% and maximum H_2O fuel dilution increased from 55.1% to 55.7%. As predicted by the chemical kinetic modelling, the rate of increase of κ_{ext} with increasing pressure for H_2-H_2O blends is expected to be higher than the H_2-CO_2 blends, and the NSD plots support this as OH* intensity fluctuations near flame detachment are reduced in the regions of highest expected turbulence (e.g. axial shear layer) compared with the H_2-CO_2 which exhibits high intensity fluctuations along the shear layer and at the burner exit nozzle.

At this thermal power scaling, the burner was not operated above 0.15 MPa due to sudden flame flashback, even at high dilution rates (> 60% Fuel Diluent), which was unexpected as the burner was operated without diluent at nearly φ = 0.25 at *P2* = 0.11 MPa. This is similarly attributed to the increased turbulence effect with increasing pressure which promotes flame propagation upstream in this low $\bar{u}$ condition.

3.2.4 ELEVATED PRESSURE (250 kW/MPa Scaling)

To extend the pressurized operation of the HPGSB-2 beyond 0.15 MPa, the thermal power scaling of 125 kW/MPa was increased to 250 kW/MPa and the burner inlet temperature was increased from 523 K to 573 K, in an effort to increase bulk velocity through the burner and reduce heat loss the rig. Thus, exhaust temperatures > 1000 K could be achieved under these conditions. Similar to the operation at 125 kW/MPa, the burner pressure was increased at a fixed φ = 0.25, with total mass flow rate scaling in proportion. At each pressure condition, the maximum diluent addition to achieve an intermittent detached flame was identified, with the results for CO_2 dilution presented in Fig. 12. Note that required steam flows could not be achieved at these conditions. In Fig. 12, mean exit nozzle velocity is within the range 46.7 < $\bar{u}$ < 48.2 m/s, with a maximum air flow of 71.5 g/s and CO_2 flow of 11.65 g/s at 0.275 MPa.

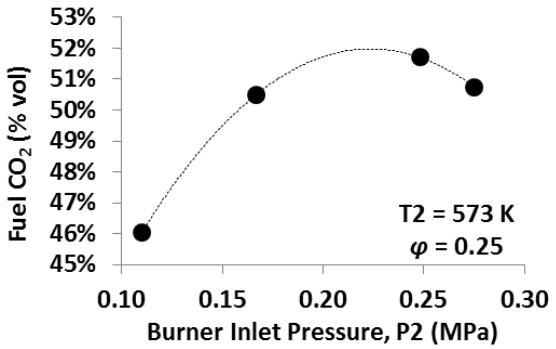

Figure 12. NON-MONOTONIC INFLUENCE OF PRESSURE ON ACHIEVABLE FUEL CO_2 (%VOL) IN H_2-AIR FLAME

As shown in Fig. 12, the maximum %vol CO_2 diluent increases from 0.11 MPa to 0.15 MPa, in agreement with the observation made in the 125 kW/bar case, although notably at lower total %vol CO_2 dilution ratios in this case. The maximum %vol CO_2 diluent increases until approximately 0.225 MPa (best fit), after which it then decreases for the 0.25 MPa and 0.275 MPa conditions. This nonmonotonic pressure dependence behavior is in agreement with the nonmonotonic behavior of dilute H_2-air κ_{ext} with increasing pressure predicted by the chemical kinetic modelling in Fig. 4. This would also be in agreement with the nonmonotonic κ_{ext} trend identified by Niemann et al. [18] for H_2-N_2-air pressurized diffusion counterflow flames. Despite the fact that the Li et al. [27] mechanism is unable to converge at these ultra-lean, dilute conditions, the trends identified at higher φ give an indication that the lean stability of dilute H_2-air flames, measured here under turbulent pressurized conditions, is increasingly influenced by thermodiffusive effects which may present important operational considerations for H_2-based GTs. Furthermore, it appears viable for the use of κ_{ext} to predict pressurized lean H_2 flame stability and requires further detailed investigation.

4. CONCLUSIONS

This study presents experimental measurements supported by chemical kinetics modelling at elevated temperature for both atmospheric (12.5 kW) and elevated pressure (125 kW/MPa and 250 kW/MPa) H_2-air, H_2-CO_2-air and H_2-H_2O-air LPM flames. Time-resolved OH* chemiluminescence characterizes the influence of fuel dilution on resulting flame stabilization from a lean detached flame limit to a rich flashback limit. Exhaust gas emissions from these ultra-lean flames were measured to prove low-NO_x operation is possible, however this at the expense of reduced combustor exhaust temperatures and increased CO emissions in the H_2-CO_2-air case. This suggests that alternative architectures or operating condition may be necessary in future work to provide practical thermal output from the burner, such as staged diffuse H_2 injection. This study provides a detailed analysis for the use of pure and dilute H_2-air in a representative GT burner geometry designed for CH_4 without any additional retrofit. The following conclusions are made:

1. Successful stabilization of pure H_2-air flames in a CH_4-air swirl burner requires operation at low equivalence ratio (φ < 0.25) with sufficiently high burner exit nozzle velocity. The stable operating equivalence ratio could be increased with sufficient levels of CO_2 dilution (up to 75 %vol fuel or 40 %vol premix) or H_2O dilution (up to 70 %vol fuel or 23 %vol premix) and turbulence ($Re_{H2} \approx 2*Re_{CH4}$). However, this comes with an associated ΔP penalty.

2. Chemical kinetics modelling of S_L, AFT, and κ_{ext} enabled identification of stable ignition points for H_2-based fuels (near 65% fuel diluent). A reduction in φ and varying amounts of fuel dilution with CO_2 or H_2O is required to reduce the pure H_2-air values within range of stable CH_4-air flames, with CO_2 influencing the reduction rate more than H_2O.

3. Pure and dilute H_2-air flames under atmospheric pressure, preheated conditions are characterized by low OH* intensity, with H_2-H_2O flames significantly lower than pure H_2-air and H_2-CO_2 flames. NSD plots of OH* intensity fluctuation under lifted flame conditions show that H_2-H_2O flames are more stable than H_2-CO_2, attributed to increased κ_{ext}.

4. Ultra-low NO_x emissions could be achieved: < 1 ppm in H_2-CO_2 cases and < 2 ppm across all other experimental conditions. This is attributed to the ultra-lean operation, which limits thermal NO_x formation. N_2O and NNH pathways may therefore be contributing. High CO emissions at low AFT in the H_2-CO_2 cases were measured, attributed to the CO_2+H = CO+OH reaction.

5. At low $\bar{u}$ corresponding to 125 kW/MPa scaling, burner operation above 0.15 MPa could not be achieved without flashback. By increasing the total mass flow through the burner at 250 kW/MPa, pressurized dilute H_2-air flames up to 0.275 MPa could be realized due to increased $\bar{u}$.

6. Maximum levels of CO_2 dilution in pressurized H_2-air flames exhibit a nonmonotonic influence with increasing *P2*, suggesting that thermodiffusive effects dominate under these highly stretched, lean conditions, in agreement with the similar nonmonotonic κ_{ext} trend with pressure identified by chemical kinetics modelling.

ACKNOWLEDGMENTS

This work was supported by funding from the FLEXIS project (Welsh European Funding Office) and the UK EPSRC Advanced Gas Turbine project (EP/M015300/1). Mr. Jack Thomas is thankfully acknowledged for his work operating and maintaining the experimental facility described herein.

REFERENCES

[1] Wezel, Ralf and Clarena Barón, Sònia. "The Turbine Industry Commits to Provide Europe with "Renewable Gas-Ready" Turbines." *Mechanical Engineering* Vol. 141 No. 9 (2019): pp. 56-57.

[2] International Energy Agency (IEA). "The Future of Hydrogen." IEA Publications, Paris (2019). Available online: https://webstore.iea.org/the-future-of-hydrogen. [Accessed November 18th, 2019]

[3] Stathopoulos, P., Kuhn, P., Wendler, J., Tanneberger, T., Terhaar, S., Paschereit, C.O., Schmalhofer, C., Griebel, P., Aigner, M. "Emissions of a Wet Premixed Flame of Natural Gas and a Mixture with Hydrogen at High Pressure." *Journal of Engineering for Gas Turbines and Power* Vol. 139 No. 4 (2017): pp. 041507. DOI 10.1115/1.4034687 https://asmedigitalcollection.asme.org/gasturbinespower/article-abstract/139/4/041507/444277/Emissions-of-a-Wet-Premixed-Flame-of-Natural-Gas

[4] Mayer, C., Sangl, J., Sattlemayer, T., Lachaux T., Bernero, S. "Study on the Operational Window of a Swirl Stabilized Syngas Burner Under Atmospheric and High Pressure Conditions." *Journal of Engineering for Gas Turbines and Power* Vol. 134 No. 3 (2012): pp. 031506. DOI 10.1115/1.4004255 https://asmedigitalcollection.asme.org/gasturbinespower/article-abstract/134/3/031506/455909/Study-on-the-Operational-Window-of-a-Swirl

[5] Sanchez, Antonio L. and Williams, Forman A. "Recent advances in understanding of flammability characteristics of hydrogen." *Progress in Energy and Combustion Science* Vol. 41 (2014): pp. 1-55. DOI 10.1016/j.pecs.2013.10.002. https://www.sciencedirect.com/science/article/pii/S0360128513000518

[6] Reichel, Thoralf G., Terhaar, Steffen, Paschereit, Oliver. "Increasing Flashback Resistance in Lean Premixed Swirl-Stabilized Hydrogen Combustion by Axial Air Injection." *Journal of Engineering for Gas Turbines and Power* Vol. 137 No. 7 (2015): pp. 071503. DOI 10.1115/1.4029119. https://asmedigitalcollection.asme.org/gasturbinespower/article-abstract/137/7/071503/373737/

[7] Strakey, P.A., Woodruff, S.D., Williams, T.C., and Schefer, R.W. "OH-Planar Fluorescence Measurements of Pressurized, Hydrogen Premixed Flames in the SimVal Combustor." *AIAA Journal* Vol. 46 No. 7 (2008): pp. 1604-1613. DOI 10.2514/1.32640. https://arc.aiaa.org/doi/10.2514/1.32640

[8] Strakey, P., Sidwell, T., and Ontko, J. "Investigation of the effects of hydrogen addition on lean extinction in a swirl stabilized combustor." *Proceedings of the Combustion Institute* Vol. 31 (2007): pp.3173-3180. DOI 10.1016/j.proci.2006.07.077. https://www.sciencedirect.com/science/article/pii/S1540748906000940

[9] Boerner, S., Funke, H.H.-W., Hendrick, P., Recker, E., and Elsing, R. "Development and Integration of a Scalable Low NO_x Combustion Chamber for a Hydrogen-Fueled Aerogas Turbine." *Progress in Propulsion Physics* Vol. 4 (2013): pp. 357-372 DOI 10.1051/eucass/201304357. https://www.eucass-proceedings.eu/articles/eucass/abs/2013/01/eucass4p357/eucass4p357.html

[10] Bower, Hannah E., Schwärzle, Andreas, Grimm, Felix, Zornek, Timo, and Kutne, Peter. "Experimental Analysis of a Micro Gas Turbine Combustor Optimized for Flexible Operation with Various Gaseous Fuel Compositions." *Journal of Engineering for Gas Turbines and Power* Vol. 142 No. 3 (2020): pp. 031015. DOI 10.1115/1.4044901. https://asmedigitalcollection.asme.org/gasturbinespower/article-abstract/142/3/031015/975754/Experimental-Analysis-of-a-Micro-Gas-Turbine

[11] Bothien, Mirko R., Ciani, Andrea, Wood, John P., and Fruechtel, Gerhard. "Toward Decarbonized Power Generation with Gas Turbines by Using Sequential Combustion for Burning Hydrogen." *Journal of Engineering for Gas Turbines and Power* Vol. 141 No. 12 (2019): pp. 121013. DOI 10.1115/1.4045256. https://asmedigitalcollection.asme.org/gasturbinespower/article-abstract/141/12/121013/1065885/

[12] Weiland, Nathan T. and Strakey, Peter A. "NO_x Reduction by Air-Side versus Fuel-Side Dilution in Hydrogen Diffusion Flame Combustors." *Journal of Engineering for Gas Turbines and Power* Vol. 132 No. 7 (2010): pp. 071504. DOI 10.1115/1.4000268. https://asmedigitalcollection.asme.org/gasturbinespower/article-abstract/132/7/071504/408835/

[13] Tanneberger, Tom, Schimek, Sebastian, Paschereit, Christian Oliver, and Stathopoulos, Panagiotis. "Efficiency Measurement Approach for a Hydrogen Oxyfuel Combustor." *Journal of Engineering for Gas Turbines and Power* Vol. 141 No. 10 (2019): pp. 101023. DOI 10.1115/1.4044779. https://asmedigitalcollection.asme.org/gasturbinespower/article-abstract/141/10/101023/975424/

[14] Masri, A.R., Dibble, R.W., and Barlow, R.S. "Chemical kinetic effects in nonpremixed flames of H_2/CO_2 fuel." *Combustion and Flame* Vol. 91 No. 3-4 (1992): pp. 285-309. DOI 10.1016/0010-2180(92)90059-X. https://www.sciencedirect.com/science/article/abs/pii/001021809290059X

[15] Cong, Tanh Le and Dagaut, Philippe. "Oxidation of H_2/CO_2 mixtures and effect of hydrogen initial concentration on the combustion of CH_4 and CH_4/CO_2 mixtures: Experiments and modelling." *Proceedings of the Combustion Institute* Vol. 32 No. 1 (2009): pp. 427-435. DOI 10.1016/j.proci.2008.05.079. https://www.sciencedirect.com/science/article/pii/S1540748908003490

[16] Kuznetsov, M., Redlinger, R., Breitung, W., Grune, J., Friedrich, A., and Ichikawa, N. "Laminar burning velocities of hydrogen-oxygen-steam mixtures at elevated temperatures and pressure." *Proceedings of the Combustion Institute* Vol. 33 No. 1 (2011): pp. 895-903. DOI 10.1016/j.proci.2010.06.050. https://www.sciencedirect.com/science/article/pii/S1540748910000763

[17] Lyu, Yajin, Qiu, Penghua, Liu, Li, Yang, Chenchen, and Sun, Shaozeng. "Effects of steam dilution on laminar flame speeds of H_2/air/H_2O mixtures at atmospheric and elevated pressures." *International Journal of Hydrogen Energy* Vol. 43 No. 15 (2018): pp. 7538-7549. DOI 10.1016/j.ijhydene.2018.02.065. https://www.sciencedirect.com/science/article/pii/S0360319918304828

[18] Niemann, U., Seshadri, K., and Williams, F.A. "Effect of pressure on structure and extinction of near-limit hydrogen counterflow diffusion flames." *Proceedings of the Combustion Institute* Vol. 34 No. 1 (2013): pp. 881-886. DOI 10.1016/j.proci.2012.06.145. https://www.sciencedirect.com/science/article/pii/S1540748912002532

[19] Göke, Sebastian, Füri, Marc, Bourque, Gilles, Bobusch, Bernhard, Göckeler, Katharina, Krüger, Oliver, Schimek, Sebastian, Terhaar, Steffen, and Paschereit, Christian Oliver. "Influence of steam dilution on the combustion of natural gas and hydrogen in premixed and rich-quench-lean combustors." *Fuel Processing Technology* Vol. 107 (2013): pp. 14-22. DOI 10.1016/j.fuproc.2012.06.019. https://www.sciencedirect.com/science/article/pii/S0378382012002408

[20] Runyon, Jon, Marsh, Richard, Bowen, Philip, Pugh, Daniel, Giles, Anthony, and Morris, Steve. "Lean methane flame stability in a premixed generic swirl burner: Isothermal flow and atmospheric combustion characterization." *Experimental Thermal and Fluid Science* Vol. 92 (2018): pp. 125-140. DOI 10.1016/j.expthermflusci.2017.11.019. https://www.sciencedirect.com/science/article/pii/S0894177717303722

[21] Runyon, Jon P., Giles, Anthony, Marsh, Richard, Pugh, Daniel, Goktepe, Burak, Bowen, Philip, and Morris, Steven. "Characterization of Additive Layer Manufacturing Swirl Burner Surface Roughness and Its Effects on Flame Stability Using High-Speed Diagnostics." *Journal of Engineering for Gas Turbines and Power* Vol. 142 No. 4 (2020): pp. 041017. DOI 10.1115/1.4044950. https://asmedigitalcollection.asme.org/gasturbinespower/article/142/4/041017/1031151/Characterization-of-Additive-Layer-Manufacturing

[22] Pugh, Daniel, Bowen, Philip, Valera-Medina, Agustin, Giles, Anthony, Runyon, Jon, and Marsh, Richard. "Influence of steam addition and elevated ambient conditions on NO_x reduction in a staged premixed swirling NH_3/H_2 flame." *Proceedings of the Combustion Institute* Vol. 37 No. 4 (2019): pp. 5401-5409. DOI 10.1016/j.proci.2018.07.091. https://www.sciencedirect.com/science/article/pii/S1540748918305091

[23] Runyon, Jon, Marsh, Richard, Pugh, Daniel, Bowen, Philip, Giles, Anthony, Morris, Steven, and Valera-Medina, Agustin. "Experimental Analysis of Confinement and Swirl Effects on Premixed CH_4-H_2 Flame Behavior in a Pressurized Generic Swirl Burner." *Proceedings of the ASME Turbo Expo 2017: Turbomachinery Technical Conference and Exposition.* GT2017-64794: pp. V04BT04A044. Charlotte, NC, June 26-30, 2017. DOI 10.1115/GT2017-64794. http://proceedings.asmedigitalcollection.asme.org/proceeding.aspx?articleid=2650020.

[24] Gaydon, A. G. *The Spectroscopy of Flames, 2nd Edition*. Chapman and Hall, London (1974).

[25] ANSYS Chemkin-Pro 2019 R2, ANSYS, Inc, Canonsburg, Pennsylvania (2019).

[26] Smith, Gregory P., Golden, David M., Frenklach, Michael, Moriarty, Nigel W., Eiteneer, Boris, Goldenberg, Mikhail, Bowman, C. Thomas, Hanson, Ronald K., Song, Soonho, Gardiner Jr., William C., Lissianski, Vitali V., and Qin, Zhiwei. "The 'GRIMech 3.0' chemical kinetic mechanism." (1999) www.me.berkeley.edu/grimech.

[27] Li, Juan, Zhao Zhenwei, Kazakov, Andrei, Chaos, Marcos, Dryer, Frederick L., and Scire Jr., James J. "A comprehensive kinetic mechanism for CO, CH_2O, and CH_3OH combustion." *International Journal of Chemical Kinetics* Vol. 39 No. 3 (2007): pp. 109-136. DOI 10.1002/kin.20218. https://onlinelibrary.wiley.com/doi/10.1002/kin.20218

[28] Shanbhogue, S.J., Sanusi, Y.S., Taamallah, S., Habib, M.A., Mokheimer, E.M.A, and Ghoniem, A.F. "Flame macrostructures, combustion instability and extinction strain scaling in swirl-stabilized premixed CH_4/H_2 combustion." *Combustion and Flame* Vol. 163 (2016): pp. 494-507. DOI 10.1016/j.combustflame.2015.10.026. https://www.sciencedirect.com/science/article/pii/S001021801500382X

[29] Hu, Erjiang, Huang, Zuohua, He, Jiajia, Jin, Chun, and Zheng, Jianjun. "Experimental and numerical study on laminar burning characteristics of premixed methane-hydrogen-air flames." *International Journal of Hydrogen* Energy Vol. 34 No. 11 (2009): pp. 4876-4888. DOI 10.1016/j.ijhydene.2009.03.058 https://www.sciencedirect.com/science/article/pii/S0360319909004868

[30] Shaddix, C. and Molina, A. "Ignition, flame stability, and char combustion in oxy-fuel combustion." *Oxy-Fuel Combustion for Power Generation and Carbon Dioxide (CO_2) Capture.* Woodhead Publishing, Cambridge (2011): pp. 101-124.

[31] Amato, Alberto, Seitzman, Jerry M., Lieuwen, Timothy C., C. and Molina, A. "Emissions from Oxyfueled or High-Exhaust Gas Recirculation Turbines." *Gas Turbine Emissions.* Cambridge University Press, New York (2013): pp. 209-234.

[32] Glarborg, Peter, Miller, James A., Ruscic, Branko, Klippenstein, Stephen J. "Modeling nitrogen chemistry in combustion." *Progress in Energy and Combustion Science* Vol. 67 (2018): pp. 31-68. DOI 10.1016/j.pecs.2018.01.002 https://www.sciencedirect.com/science/article/pii/S0360128517301600

[33] Pavri, R., Moore, G. D. "Gas Turbine Emissions and Control." General Electric Power Systems (2001). Report No. GER 4211.

[34] Glarborg, Peter and Bentzen, Line L. B. "Chemical Effects of a High CO_2 Concentration in Oxy-Fuel Combustion of Methane." *Energy and Fuels* Vol. 22 No. 1 (2008): pp. 291-296. DOI 10.1021/ef7005854. https://pubs.acs.org/doi/10.1021/ef7005854

